Hindawi
Mathematical Problems in Engineering
Volume 2018, Article ID 9835341, 14 pages
https://doi.org/10.1155/2018/9835341

Research Article

A Method for Estimating the Surface Roughness of Rock Discontinuities

Yi Cai,[1] **Hui-ming Tang**,[1,2] **Ding-jian Wang**,[1] **and Tao Wen**[1]

[1]*Faculty of Engineering, China University of Geosciences, Wuhan 430074, China*
[2]*Three Gorges Research Center for Geo-Hazard, Ministry of Education, Wuhan 430074, China*

Correspondence should be addressed to Hui-ming Tang; tanghm@cug.edu.cn

Received 19 October 2017; Revised 26 January 2018; Accepted 8 February 2018; Published 18 March 2018

Academic Editor: Fabrizio Greco

The primary objective of this study is to develop a parameter with a clear physical meaning to estimate the surface roughness of rock discontinuities. This parameter must be closely related to the shear strength of rock discontinuities. The first part of this study focuses on defining and computing this parameter. The estimation formula for the shear strength of a triangle within a discontinuity surface is derived based on Patton's model. The parameter, namely, the index of roughness (I_R), is then proposed to quantitatively estimate discontinuity roughness. Based on laser scanning techniques, digital models of discontinuities and discontinuity profiles are constructed, and then their corresponding I_R values are computed. In the second part of this study, the computational processes and estimated effects of the two-dimensional (2D) and three-dimensional (3D) I_R values of the discontinuities are illustrated through several applications. Results show that the 2D and 3D I_R values of these discontinuities indicate anisotropy and sampling interval effects. In addition, a strong linear correlation is detected between I_R and the joint roughness coefficient (JRC) for seventy-four profiles and eleven discontinuity specimens, respectively. Finally, the proposed method, back analysis method, root mean square (Z_2) method, and Grasselli's method are compared to study the use of the parameter I_R.

1. Introduction

Rock masses usually contain significant discontinuities such as joints, faults, bedding planes, fractures, and other mechanical defects. The surface roughness of rock discontinuities plays an important role in the mechanical properties of rocks, including the shear strength and deformation [1–4], and can also directly affect the seepage behaviors of discontinuities [5, 6]. One of the purposes of studying discontinuities is to accurately and quickly estimate their quantitative roughness to then assess their shear strength. Thus, researchers have attempted to develop roughness estimation methods for discontinuities.

Myers [7] proposed the root mean square parameter Z_2 to quantitatively describe the roughness of discontinuity profiles:

$$Z_2 = \sqrt{\frac{1}{L}\int_{x=0}^{x=L}\left(\frac{dy}{dx}\right)^2 dx} \approx \sqrt{\frac{1}{M}\sum_{i=1}^{M}\left(\frac{y_{i+1}-y_i}{D}\right)^2} = \sqrt{\frac{1}{M}}\sqrt{\sum_{i=1}^{M}(\tan\theta_i)^2}, \quad (1)$$

where the x- and y-axes are the extension and fluctuation directions of the profile, respectively; L is the length of the horizontal projection of the profile; D is the horizontal sampling interval; M is the number of discrete line segments of the profile; and θ is the dip angle of a line segment between two adjacent points. Barton [1] proposed the joint roughness coefficient (JRC) to describe the surface roughness of a discontinuity, and ten typical profiles were presented by Barton and Choubey [2]. The structure function (SF) and roughness profile index (R_P) were also proposed to quantitatively evaluate surface roughness [8, 9]. Later, correlations between the JRC and other parameters, such as Z_2, SF, and R_P, have been investigated by researchers [10–13]. Recently, several other methods have been proposed to quantify discontinuity roughness. Grasselli and his colleagues proposed a roughness estimation parameter $\theta^*_{\max}/(C_G+1)$ based on the statistical analysis of the potential contact areas [14–17]. Ye et al. [18] proposed a JRC estimation method based on neutrosophic functions. Moreover, according to previous studies, several improved roughness parameters have been proposed.

For example, regarding Z_2, Belem et al. [19] proposed a formula for calculating the 3D root mean square (Z_2), and Zhang et al. [20] suggested a modified root mean square (Z_2') that can describe the anisotropies of profile roughness. Additionally, fractal theory was used to estimate the roughness of discontinuities [21–23]. Meanwhile, the scale effect, sampling interval effect, and anisotropy of discontinuity roughness were studied by researchers. For example, Barton and Choubey [2] first emphasized the existence of a scale effect during discontinuity roughness estimations, and Yu and Vayssade [12] noted that roughness parameters, such as Z_2 and SF, were sensitive to the sampling interval.

In conclusion, existing discontinuity roughness estimation methods can be mainly subdivided into three categories: empirical methods [1, 2], statistical methods [7–20], and fractal analysis methods [21–23]. Although these methods can effectively describe the morphological features of discontinuities, they may have the following limitations: (1) the roughness estimated by an empirical method may be subjective and (2) most statistical methods and fractal analysis methods estimate the roughness without closely incorporating their shear failure mechanisms, making the physical meanings of these roughness parameters unclear and resulting in a weak relationship between the roughness parameters and shear strength of the discontinuities. For example, Z_2, which was proposed by Myers [7], can represent the root mean square of the tangential values of all of the tooth dip angles (i.e., $\tan(\theta)$) without considering the shear directions (see (1)). However, the relationship between the tooth dip angle (θ) and the tooth shear strength (τ) does not conform to an exact tangential function (see (2) proposed by Patton [24]):

$$\tau = \sigma \tan\left(\phi_b + \theta\right), \tag{2}$$

where σ and ϕ_b are the normal stress and the basic friction angle, respectively. Therefore, the shear strength of discontinuities estimated with Z_2 cannot directly reflect the influence of the basic friction angle (ϕ_b). In other words, the relationship between Z_2 and the shear strength of discontinuities is not well established. As another example, Grasselli's method can effectively estimate the 3D discontinuity roughness using the parameter ${\theta^*}_{\max}/(C_G+1)$; however, the physical meaning of this parameter is unclear [25, 26].

A strong connection between the roughness parameter and the shear strength of discontinuities should be established and could contribute to building a shear strength model of discontinuities. Therefore, based on the shear failure mechanism of discontinuities, a formula for the shear strength of a triangle within a discontinuity surface is derived from Patton's model, and the roughness estimation parameter, index of roughness (I_R), and its calculation are then presented. In addition, the calculation procedure and effects of the proposed method are presented using applied examples. Finally, the rationality of the new method is analyzed based on comparisons with other methods.

2. Mechanical Basis

The normal stress directly affects the shear failure mechanism of discontinuities. Jaeger [27] noted that some of the asperities on a discontinuity can be sheared off under low normal stress and that failures under only dilation or shear are both extreme cases. Pereira and de Freitas [28] drew similar conclusions in their study of the shear failure mechanism of sandstone with teeth-discontinuities. Therefore, for natural discontinuities, when the normal stress is low, the dilation effect is dominant, and when the normal stress is high, shear failure of asperities is dominant over dilation.

In addition, when materials fill the discontinuity gap, the shear resistance of the discontinuity can be affected by the properties of these filling materials. To simplify the discontinuities in this study, we hypothesize that the discontinuities are well-mated and that no gaps are present along them.

2.1. Shear Failure Mechanism of a Regular-Teeth-Discontinuity. The teeth-discontinuity model proposed by Patton [24] is shown in Figure 1(a). The asperity features include the number of teeth and their dip angles (θ) and heights (h). In this paper, Patton's teeth-discontinuity model, which uses the same parameters θ and h for all of the teeth, is defined as the regular-teeth-discontinuity (RTD) model. Based on the RTD specimens, Patton studied the relation between the shear strength (τ) and the dip angle (θ). Figure 1(b) shows a force analysis of a single tooth from the RTD model under a normal stress (σ). The basic friction angle of the discontinuity is ϕ_b, and the normal and shear stresses on a tooth surface are σ_n and τ_n, respectively.

$$\begin{aligned} \sigma_n &= \tau \sin\theta + \sigma \cos\theta \\ \tau_n &= \tau \cos\theta - \sigma \sin\theta. \end{aligned} \tag{3}$$

By assuming that the shear strength τ of the RTD is consistent with the Coulomb-Navier criterion (4) and inserting the corresponding parameters of (3) into (4), (2) can be obtained.

$$\tau_n = \sigma_n \tan\phi_b. \tag{4}$$

Patton studied the shear strength envelopes of RTD specimens with different teeth inclinations, as illustrated in Figure 2(a), where ϕ_r is the residual friction angle of the RTD specimen. Additional studies indicate that (2) can be applied to the shear strength calculations of RTD models only at low normal stress. When the normal stress σ exceeds σ_T (Figure 2(b)), the shear strength envelope will experience a transition. After the transition, the shear strength τ of the RTD is calculated by

$$\tau = \sigma \tan\phi_r + C, \tag{5}$$

where C is the cohesion. Therefore, a bilinear model (Patton's model) for calculating the shear strength of the RTD model is given as

$$\tau = \sigma \tan\left(\phi_b + \theta\right), \quad \sigma \le \sigma_T \tag{6a}$$

$$\tau = \sigma \tan\left(\phi_r\right) + C, \quad \sigma > \sigma_T. \tag{6b}$$

2.2. Shear Failure Mechanism of an Irregular-Teeth-Discontinuity. Discontinuities in natural rock masses are complex. For engineering purposes, additional research on the

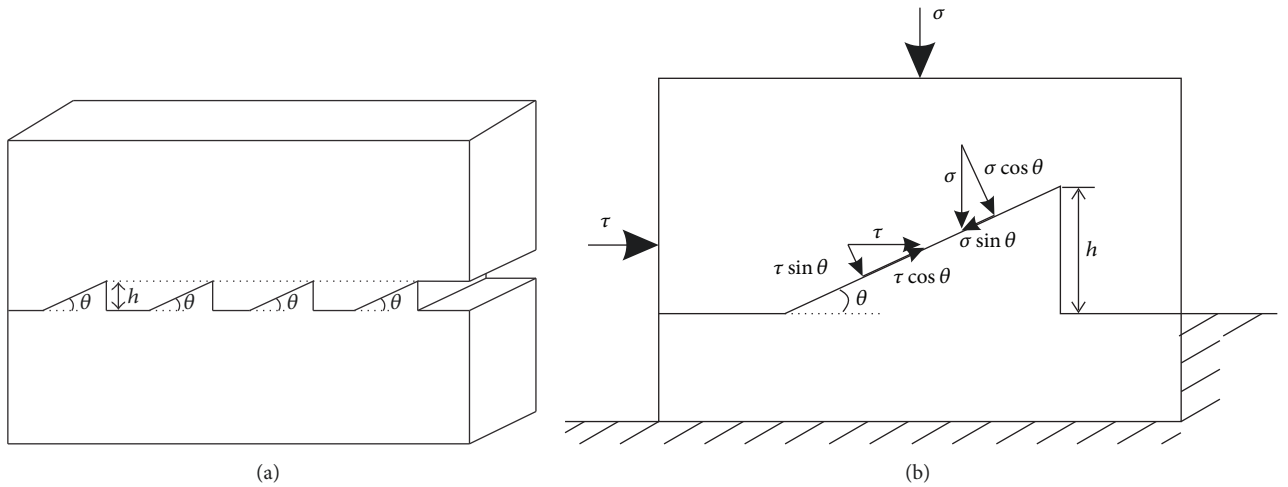

Figure 1: RTD model and its shear force analysis: (a) RTD model (modified from Patton [24]); (b) shear force analysis of a single tooth.

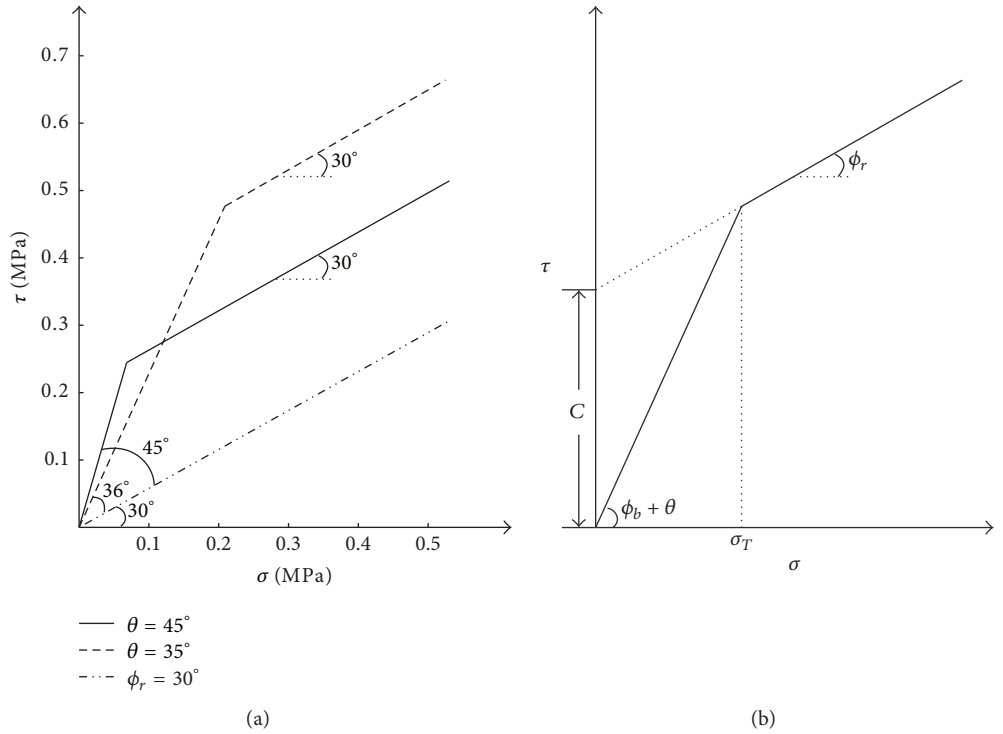

Figure 2: Shear strength envelopes of the RTD models: (a) failure envelopes of the RTD models with different asperity angles (modified from Patton [24]); (b) typical failure envelope of the RTD model.

irregular-teeth-discontinuity (ITD) model, which is defined as a teeth-discontinuity model with different tooth inclinations, is very important. Figure 3(a) shows a basic overview of the ITD model, in which the tooth base length and basic friction angle are constant and labeled D and ϕ_b, respectively. All of the tooth base lengths in the ITD are equal to D; this conforms to the data acquisition method, which uses a 3D laser scanning technique over equal intervals.

The equation $\sigma_T = C/[\tan(\phi_b + \theta) - \tan\phi_r]$ can be derived easily from (6a) and (6b). In the RTD, the value of σ_T decreases as the tooth dip angle (θ) increases (Figure 2(a)). Thus, as shown in Figure 3, the shear failure law of the ITD teeth under normal stress (σ) can be determined as follows: (1) for a tooth with a low dip angle (θ), when the σ_T value of the tooth is greater than σ, the shear strength of the tooth can be calculated using (6a); and (2) for a tooth with a high dip angle θ, when the σ_T value of the tooth is less than σ, the shear strength of the tooth can be calculated using (6b). Therefore, when shear tests of an ITD model are conducted at a low normal stress, most of the teeth, which are at various dip angles, are damaged via the dilation effect. Consequently, the failure mechanism of every tooth is regarded

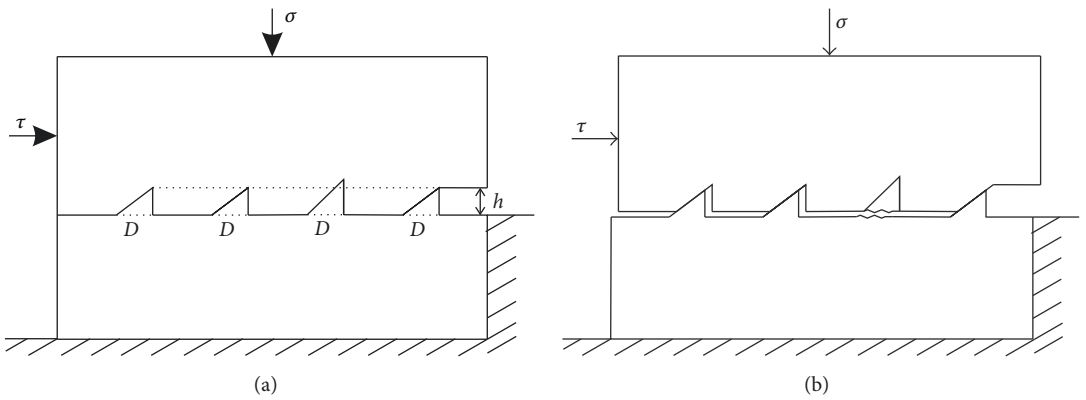

Figure 3: ITD model and its shear failure mechanism: (a) before shear failure; (b) after shear failure.

as a dilation failure, which may be an inaccurate assumption for the following reasons: (1) when $\phi_b + \theta$ of a tooth is equal to or greater than 90°, the shear strength of the tooth may be infinite or negative; and (2) when $\phi_b + \theta$ of a tooth approaches 90°, the shear strength of the tooth may exceed the shear strength that is initially required to shear off the tooth.

For an ITD model with a normal stress (σ), the shear strength of every tooth can be calculated using (6a) or (6b). However, only (6a) reflects the influences of the dip angles on the shear strength of the ITD teeth, whereas (6b) does not. Therefore, to better represent the influences of the tooth dip angles on the shear resistances in ITD models, this study assumes that the shear tests are performed with ITD models under low normal stress conditions, such that most of the teeth, at varying dip angles, experience dilation failure. Similarly, many studies on the roughness and shear strength of discontinuities are conducted under a low normal load [2, 23]. Based on this assumption, the shear strength (τ_0) of every tooth in the ITD can be quickly estimated using

$$\begin{aligned} \tau_0 &= \min\left(\tau^*, \tau'\right) \quad \text{with } \tau^* \geq 0 \\ \tau_0 &= \tau' \quad \text{with } \tau^* < 0 \\ \tau^* &= \sigma \tan\left(\phi_b + \theta\right) \\ \tau' &= \sigma \tan \phi_r + C, \end{aligned} \tag{7}$$

where τ^* and τ' are the shear strength of the tooth damaged by the dilation failure and the shear strength threshold of the tooth sheared off. When the shear stress of a tooth is greater than τ', the tooth can be sheared off; otherwise, the tooth may be damaged by the dilation effect only. In addition, according to Patton [24], the following assumption can be made: $\phi_r = \phi_b$.

2.3. Shear Strength of a Tooth Surface in Three Dimensions. In 3D roughness characterization, a discontinuity surface can be discretized into adjacent triangles, with each triangle orientation uniquely identified by its dip angle (θ) and azimuth angle (α) (Figure 4). θ is the angle between the shear plane and the triangle. α is the angle between the true dip vector

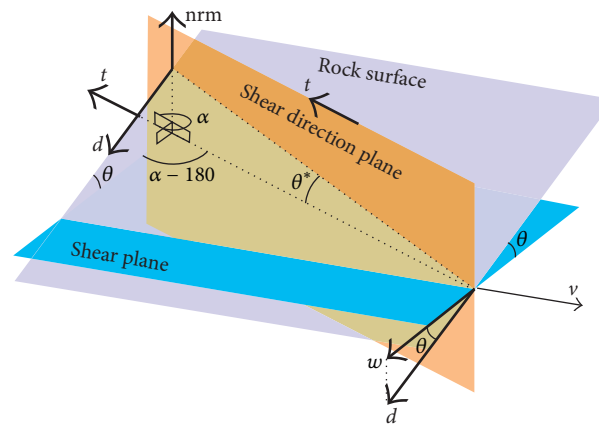

Figure 4: Apparent dip angle θ^* measured along the shear direction with respect to the shear plane [14].

(**d**) projected on the shear plane (**w**) and the shear vector (**t**) and is measured clockwise from **t**. The apparent dip angle (θ^*) describes the apparent inclination of every triangle with respect to the chosen shear direction and can be calculated using (8) given by Grasselli et al. [14].

$$\tan \theta^* = -\tan \theta \cos \alpha. \tag{8}$$

The variation in the potential contact area (A_{θ^*}) versus the apparent dip angle (θ^*) is analyzed, and the following equation was adopted by Grasselli et al. [14] to fit the data:

$$A_{\theta^*} = A_0 \left[\frac{\theta^*_{\max} - \theta^*}{\theta^*_{\max}}\right]^{C_G}, \tag{9}$$

where A_0 is the maximum potential contact area, $\theta^*_{\max}$ is the maximum apparent dip angle with respect to the chosen shear direction, and C_G is a roughness parameter. Finally, Grasselli and his colleagues used the term $\theta^*_{\max}/(C_G + 1)$ to effectively describe the discontinuity roughness [14, 25, 26].

In Grasselli's method, the potential contact triangles with equal apparent dip angle (θ^*) were regarded as the same, and their areas were calculated and summed together. In this paper, we hypothesize that the shear strengths of the potential

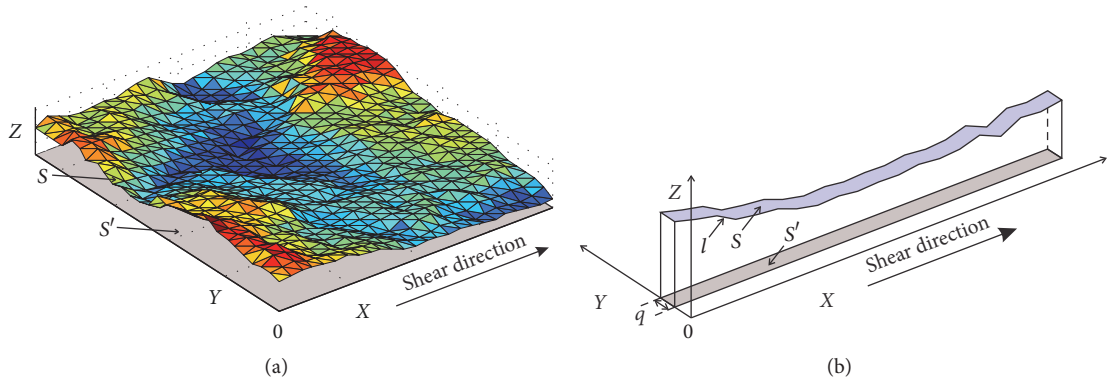

FIGURE 5: Discontinuity model for the definition and calculation of I_R: (a) modeling of the discontinuity surface; (b) modeling of the discontinuity profile.

contact triangles with the same apparent dip angles are equal. Based on this hypothesis, the shear strength (τ_0) of a potential contact triangle with the apparent dip angle (θ^*) can be estimated using the triangle whose dip angle (θ) is equal to θ^* by (7), as follows:

$$\begin{aligned} \tau_0 &= \min\left(\tau^*, \tau'\right) \quad \text{with } \tau^* \geq 0 \\ \tau_0 &= \tau' \quad \text{with } \tau^* < 0 \\ \tau^* &= \sigma \tan\left(\phi_b + \theta^*\right) \\ \tau' &= \sigma \tan \phi_r + C. \end{aligned} \tag{10}$$

3. Definition and Calculation of I_R

The data acquisition process provides a basis for estimating the roughness of discontinuities. The surface asperity features can be directly measured by several contact and noncontact tools and techniques. Contact techniques include a needle contour [2, 29] and an automatic profiler [30]; noncontact techniques include photogrammetry [11, 31] and 3D laser scanning [32, 33].

3.1. Proposing I_R. A strong connection between the roughness parameter and the shear strength of the discontinuities can contribute to establishing a shear strength model of discontinuities. Therefore, this paper proposes a new parameter, I_R, regarding the shear failure mechanism of discontinuities. For a discontinuity S under a normal stress σ ($\sigma \neq 0$) and a shear stress τ (Figure 5), the I_R value of S with respect to the shear direction of τ can be calculated by the following expression:

$$I_R = \frac{F_T}{F_H}, \tag{11}$$

where F_T is the accumulated antishearing force of all of the potential contact areas in S and F_H is the antishearing force of the horizontal projection plane of S, which is written as S'. The basic friction angles of S and S' are both ϕ_b.

The parameter I_R represents the antishearing ability per unit area of S. The antishearing force is influenced or controlled by the roughness, normal stress, and mechanical properties of the discontinuities. If the normal stress and the mechanical properties of S are all set to constant values, the greater the roughness, the higher the I_R value. To make I_R represent only the roughness of the discontinuities, an empirical equation for the I_R calculation without considering the influence of the mechanical parameters needs to be studied based on (11) (see Section 3.2). The parameter I_R calculated only by the empirical equation can be considered an index of roughness for discontinuities. Additionally, the anisotropy of the discontinuity roughness can be considered using I_R.

3.2. Calculation of I_R. The calculation procedure of I_R is outlined according to Figure 5.

(1) Data Acquisition and Modeling. A discontinuity model is built in a 3D rectangular coordinate system. The x- and y-axes are located on the horizontal plane, and the azimuths of the positive x- and y-axes are 90° and 0° (360°), respectively. The z-axis denotes the elevation. The discontinuity and its horizontal projection plane are denoted as S and S', respectively. The detailed processes can be described as follows: first, obtain the point cloud data of the discontinuity S at a sampling interval D using the 3D laser scanning technique; second, build up the point cloud map with the sequential discrete points; finally, construct the model of the discontinuity surface S with many sequential discrete triangles, denoted as S_k ($k = 1, 2, 3, \ldots$).

(2) Identifying All of the Potential Contact Triangles within the S Surface and Then Calculating Their Accumulated Antishearing Force. This process is explained using the triangle S_k as an example.

First, identify whether S_k is a potential contact triangle. S_k is considered a potential contact triangle only when its apparent angle (θ^*), calculated by (8), is between 0° and 90°. Additionally, assume that S_k, which is also written as S_j, is the jth potential contact triangle of S. Then, according to (10), the antishearing force of S_j is written as F_j and can be estimated using

$$\begin{aligned} F_j &= \tau_j^* A_j^* \quad \text{with } 0 \leq \tau_j^* \leq \tau_j' \\ F_j &= \tau_j' A_j' \quad \text{with } \tau_j^* < 0 \text{ or } \tau_j^* > \tau_j' \end{aligned}$$

$$\tau_j^* = \sigma \tan\left(\phi_b + \theta_j^*\right)$$
$$\tau_j' = \sigma \tan \phi_b + C, \tag{12}$$

where A_j^* and A_j' are the area and horizontal projection area of S_j, respectively; τ_j^* and τ_j' are the shear strength of S_j damaged by the dilation failure and the shear strength threshold of S_j before it is sheared off along its root, respectively; and θ_j^* is the apparent dip angle of S_j. Because of the differences between the teeth in ITD models and the triangles that describe a natural discontinuity, each triangle is assumed to be independent of the others and can be sheared off along its root.

After calculating the antishearing force of every potential contact triangle of S, the accumulated antishearing force of all of the potential contact triangles of S is written as F_T and can be calculated using

$$F_T = \sum_{j=1}^{n} F_j, \tag{13}$$

where n is the number of potential contact triangles of S.

(3) Calculation of the Antishearing Force (F_H) of S'. For I_R to represent the antishearing ability per unit area of S, F_H is introduced:

$$F_H = A_H \tau_H = A_H \sigma \tan \phi_b, \tag{14}$$

where τ_H and A_H are the shear strength and area of S', respectively.

(4) The I_R Calculation of S. Based on (11)–(14), the parameter I_R of S with respect to the chosen shear direction can be calculated using (15) ($\lambda = C/\sigma$).

$$I_R = \frac{F_T}{F_H} = \frac{\sum_{j=1}^{n} F_j}{A_H \sigma \tan \phi_b} = \frac{\sum_{j=1}^{n} R_j}{A_H \tan \phi_b}$$
$$R_j = A_j^* \tan\left(\phi_b + \theta_j^*\right), \quad \text{with } 0 \le \tau_j^* \le \tau_j' \tag{15}$$
$$R_j = A_j' \left(\tan \phi_b + \lambda\right), \quad \text{with } \tau_j^* < 0 \text{ or } \tau_j^* > \tau_j'.$$

The parameters used for the I_R calculation can be classified into two categories; the first category includes θ_j^*, A_j^* (A_j'), A_H, and n, which represent the geometric features of the discontinuities, and the second category includes ϕ_b and λ (C/σ), which represent the mechanical properties of the discontinuities. The parameters of the first category can be obtained from discontinuity models. Additionally, as mentioned in Section 3.1, for I_R to represent only the roughness of the discontinuities, an empirical equation for the I_R calculation without considering the influence of the mechanical parameters needs to be studied based on (15). Consequently, we set the mechanical parameters (ϕ_b and λ) as constants for (15) and then analyze the roughness estimation effects based on I_R. Specifically, for the basic friction angle (ϕ_b), ϕ_b of unweathered rock discontinuities are between 25° and 35° [2]; therefore, the value of ϕ_b is 30° in this paper. For the parameter λ, seventy-four profiles from the literature are chosen to study the appropriate value of λ for a wide applicability of the empirical equation. Analyses indicate that I_R calculated by (15) with $\phi_b = 30°$ and $\lambda = 3$ can describe the discontinuity roughness well (see Section 4.1). Thus, (15) with $\phi_b = 30°$ and $\lambda = 3$ is the proposed empirical equation for calculating I_R.

Additionally, the I_R-based roughness estimation method can be applied to 2D discontinuities. Taking a profile (l) as an example (Figure 5(b)), we translate the profile l along the y-axis at a width of q to form a discontinuity surface, denoted as S. And then I_R of the surface S can be estimated as mentioned above. Furthermore, it can be proven that there is no influence of the q value on the I_R estimation results. Therefore, the value of q is taken as D for modeling discontinuity profiles in this paper.

4. Results and Discussion for Applications

4.1. 2D I_R for Seventy-Four Profiles. In addition to the ten typical profiles proposed by Barton and Choubey [2] (Figure 6(a)), this study makes use of another sixty-four profiles from Bandis [34]. The seventy-four profiles were proposed with their JRC values estimated by back analyses of shear tests. The projected lengths of the chosen profiles range from 72 to 104 mm, and their JRC values range from 0.4 to 20. Furthermore, the rocks that these profiles were collected from cover a wide variety of rock types, including slate, granite, gneiss, sandstone, siltstone, and limestone. Therefore, the seventy-four profiles are representative to study the processes and effects of I_R.

I_R of each profile is calculated as follows: First, extract discrete points with coordinates along the profile at a horizontal interval of $D = 0.25$ mm. The profile model is then built (an example is given in Figure 6(b)). Finally, the calculation is performed following Section 3.2. For comparison, each profile model extends in the positive x direction, and the minimum coordinates of the profile along the x- and z-axes are zero.

Before calculating I_R, the primary task is to determine the proper value of λ. I_R of each profile is estimated under different values of λ (i.e., 1, 2, 2.5, 2.6, etc.). Then, the linear regression analyses between I_R and JRC for seventy-four profiles are conducted with different λ. The results, shown in Figure 7(a), indicate that there is a high linear correlation between the parameters I_R and JRC under different λ. Furthermore, the correlation coefficient (R) first increases and then decreases with increasing λ and reaches a maximum when $\lambda = 3$. The reason for decrease of R with increasing λ ($\lambda > 3$) is that the I_R values of some profiles may monotonously increase with increasing λ, that is, because the antishearing ability of the triangle may be magnified by increasing λ. For example, the antishearing ability of a triangle in which $(\phi_b + \theta^*) \ge 90$ increases with λ (see (15)). Thus, λ is set to 3, and the distribution of I_R in relation to JRC for the seventy-four profiles is plotted in Figure 7(b).

The corresponding shear directions of the JRC values for sixty-four profiles are known, while those for the ten typical

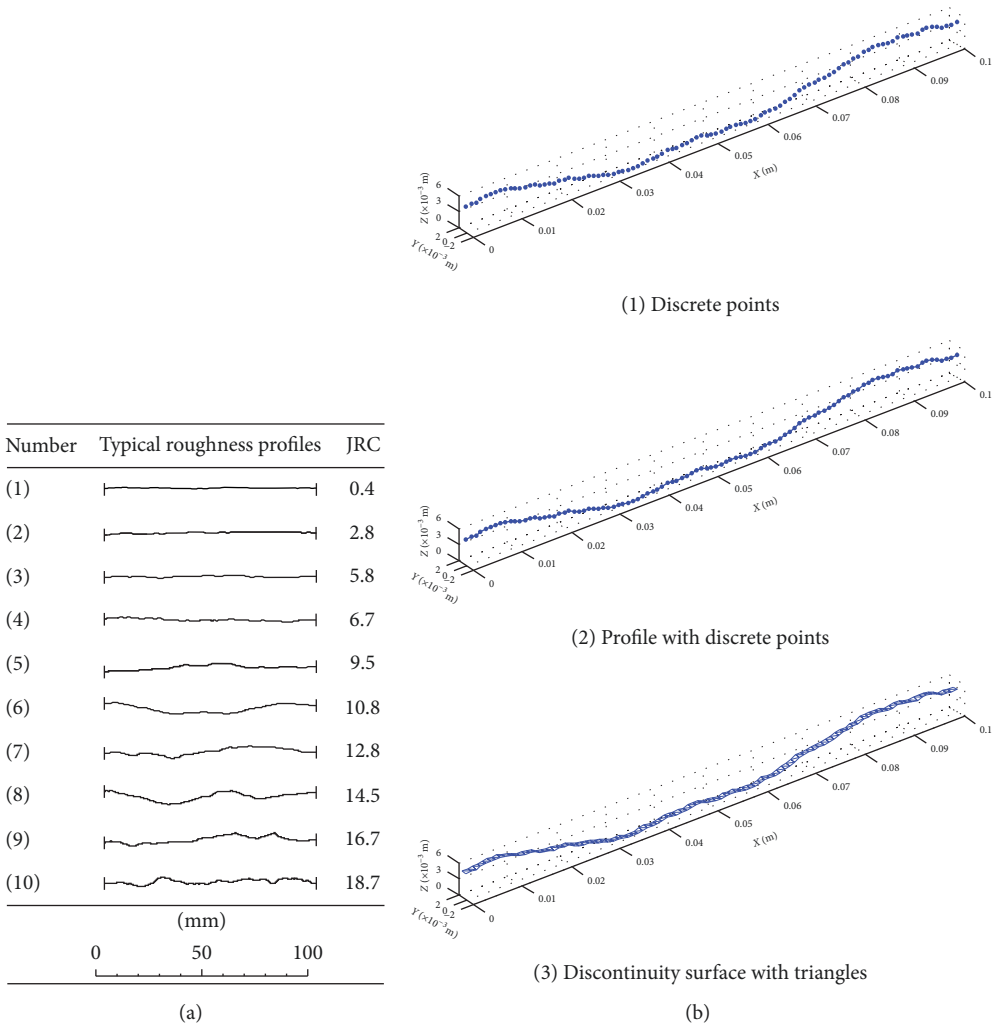

FIGURE 6: Typical profiles and their models: (a) typical profiles with JRC values calculated by back analyses [2]; (b) process of modeling a profile (JRC = 10.8; D = 1 mm).

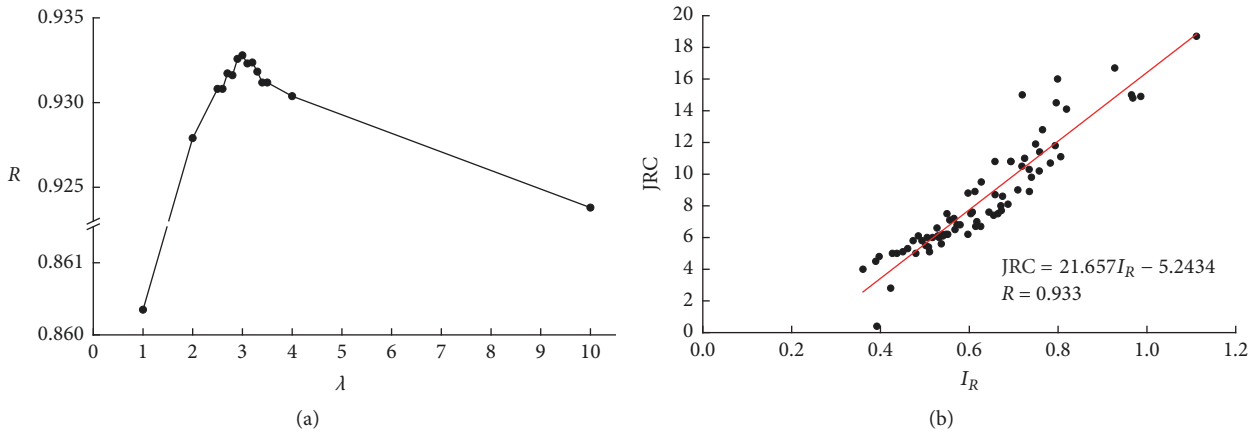

FIGURE 7: Linear correlation between I_R and JRC across the seventy-four profiles (D = 0.25 mm): (a) variation in the linear correlation coefficient (R) between I_R and JRC with λ; (b) distribution of I_R in relation to JRC for the seventy-four profiles.

Table 1: I_R values for different values of D for typical profiles.

JRC	I_R (D = 0.25 mm)			I_R (D = 0.5 mm)		
	→	←	Average	→	←	Average
0.4	0.4068	0.3771	0.3920	0.3195	0.3001	0.3098
2.8	0.4611	0.3855	0.4233	0.4414	0.3468	0.3941
5.8	0.5069	0.4406	0.4737	0.4474	0.3966	0.4220
6.7	0.6041	0.6253	0.6147	0.6035	0.6144	0.6089
9.5	0.7034	0.5507	0.6271	0.6641	0.5112	0.5877
10.8	0.6364	0.6797	0.6580	0.6195	0.6497	0.6346
12.8	0.8196	0.7106	0.7651	0.7629	0.6876	0.7253
14.5	0.7879	0.8039	0.7959	0.7614	0.7742	0.7678
16.7	1.0236	0.8319	0.9277	0.9640	0.7612	0.8626
18.7	1.0718	1.1521	1.1119	1.0596	1.1075	1.0836

→ and ← represent the I_R values with respect to the shear directions along the positive and negative x-axis, respectively.

profiles are not. Therefore, for the sixty-four profiles, the I_R value of each profile is calculated for the known shear direction; for the ten typical profiles, the average value of I_R for each profile in the two shear directions is calculated. Furthermore, the value of λ is set to 3 based on the I_R estimation results of only the seventy-four profiles; in future studies, λ may be accurately modified in engineering practices.

Additionally, the influences of the sampling interval D on the I_R evaluation results are investigated. The I_R values of the typical profiles are then estimated with D = 0.5 mm; the calculation results are listed in Table 1. According to Table 1, the histograms of I_R with JRC for the typical profiles and different D values are plotted in Figure 8. Clearly, the sampling interval D affects the I_R estimation results. In addition, I_R generally increases with decreasing D, which is consistent with the research results of Yu and Vayssade [12].

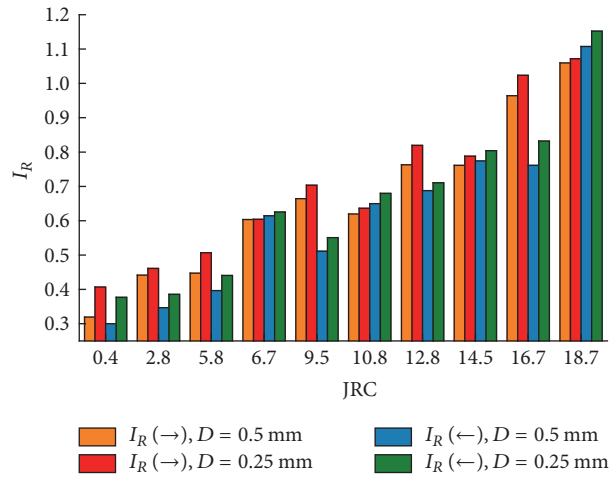

Figure 8: I_R values of the ten typical profiles with different values of D.

4.2. 3D I_R for Natural Discontinuities. Jiweishan mountain is located approximately 1 km southeast of Tiekuang Township, in Wulong County, Chongqing, China (Figure 9(a)). A rockslide occurred on Jiweishan mountain on June 5, 2009, and it exposed large-scale discontinuities and provided suitable conditions for data acquisition of the natural discontinuities. In Figure 9(b), the light purple area indicates the source area of the Jiweishan rockslide, and the yellow circle shows the sampling location. Eleven well-mated discontinuity samples were collected, including six limestone discontinuities ($L1$~$L6$) and five shale discontinuities ($S1$~$S6$). The horizontal projected area of the eleven samples is between 82 and 115 cm^2. The basic friction angle (ϕ_b), uniaxial compressive strength (σ_c), cohesion (C), and internal friction angle (ϕ) of these rock discontinuities are shown in Table 2. We estimate the roughness of these samples based on the proposed method and the back analysis method as follows.

(1) Sample Preparation and Data Acquisition. First, the discontinuity samples were embedded in cement mortar within a shear box, and the size of a top/bottom part of the box is 15 cm × 15 cm × 7.5 cm. Then, after 28 days of curing, eleven discontinuity specimens were prepared. Finally, a 3D laser scanning technique was applied to the eleven samples, using a PowerScan-Pro type 3D laser scanning apparatus supported by Vision3D Technology Co., Ltd., Wuhan (Figure 10(a)). The sampling interval D was set to 0.3 mm. 3D point cloud data of only one surface was collected for each discontinuity specimen, and the values of I_R and JRC were calculated from that surface.

(2) JRC Calculation. In this study, the JRC values of discontinuities were calculated by back analyses based on direct shear tests according to

$$\mathrm{JRC} = \frac{[\arctan(\tau/\sigma) - \phi_b]}{\log_{10}(\mathrm{JCS}/\sigma)}, \tag{16}$$

where JCS is the joint wall compressive strength and τ is the peak shear strength measured from shear tests [2]. First, all of the direct shear tests were conducted under constant normal load conditions using servo-hydraulic direct shear test equipment at the rock mechanics laboratory of the China University of Geosciences (Figure 10(b)). The shear velocity was set to 0.5 mm/min. Each shear test ended when the

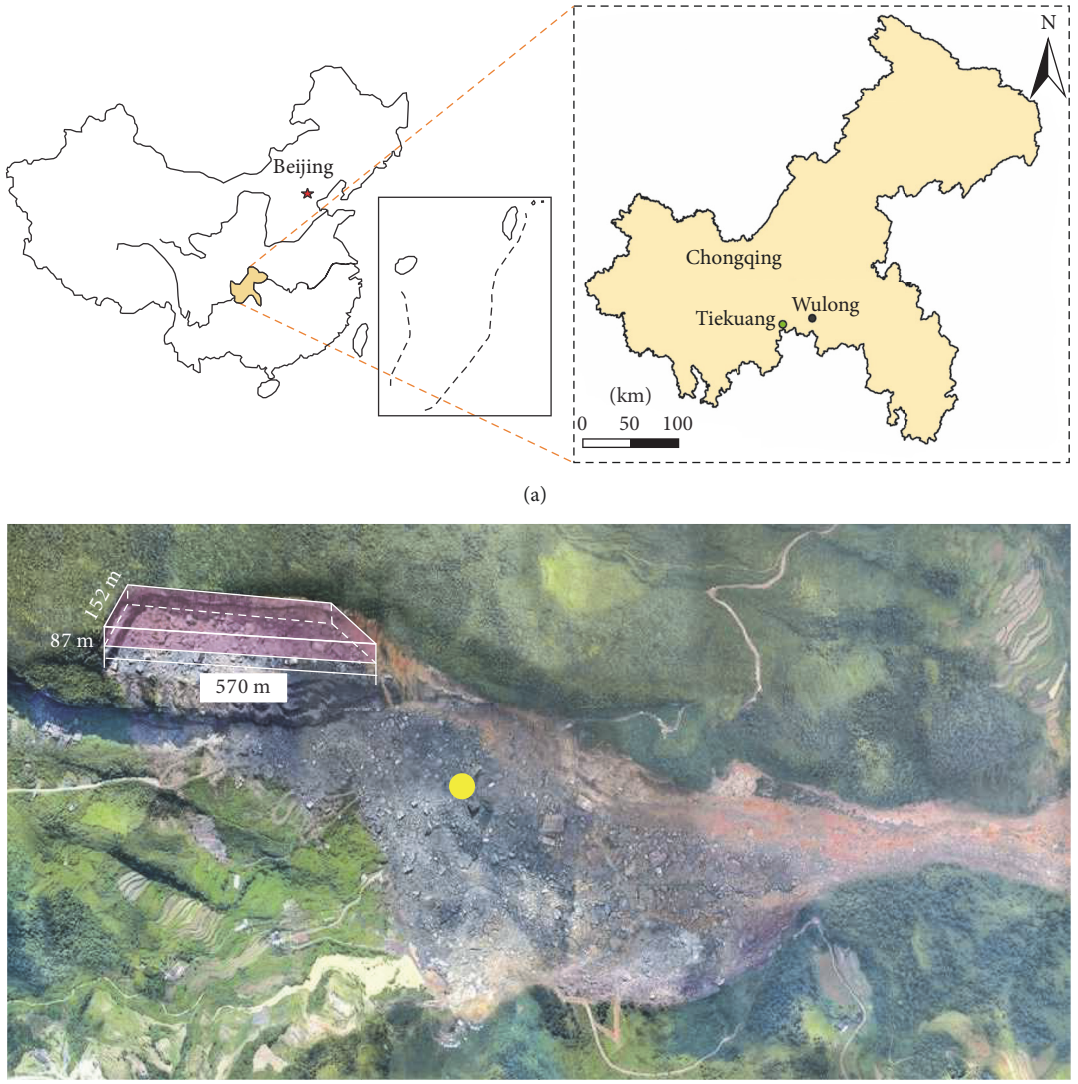

Figure 9: (a) Geographic location and (b) sampling point of the Jiweishan rockslide.

Table 2: Mechanical properties of the eleven discontinuity samples.

Rock types	ϕ_b (°)	σ_c (MPa)	C (MPa)	ϕ (°)
Limestone	30.5	90.6	11.2	44.6
Shale	22.8	36.6	5.3	33.3

residual strength was reached or the sample failed. During the experiments, each shear sample was subjected to a selected normal stress in the range of 0.48 to 3.75 MPa (Table 3). Then, a total of eleven direct shear tests were performed, and the corresponding peak shear strengths (τ) were measured. Finally, the JRC value of each sample was calculated by (16), in which the JCS was replaced by σ_c [2]. The results are listed in Table 3.

(3) I_R Calculation. Based on the point cloud data, models of the eleven discontinuity specimens are developed; some of the modeling process is shown in Figure 11. As discussed in Section 3.2, the azimuths of the positive directions of the x- and y-axes are 90° and 0° (360°), respectively. The shear directions in the laboratory are all along the positive x-axis, so we calculate the I_R value corresponding to the positive x-axis for each specimen model (D = 0.3 mm). The results are shown in Table 3.

Based on the surface data and shear test results of the eleven specimens, the estimation effects of the proposed method are analyzed as follows.

(1) Correlation of I_R with Test Shear Strength. According to Table 3, the graph of I_R versus JRC across theeleven discontinuity specimens is plotted in Figure 12. A strong linear correlation of the roughness estimation results between the

Table 3: Results of the shear tests and roughness estimations for the eleven discontinuity specimens.

Specimens	σ (MPa)	τ (MPa)	JRC	I_R
$L1$	0.48	0.92	14.02	0.82
$L2$	0.83	1.03	10.21	0.71
$L3$	0.93	0.68	2.94	0.51
$L4$	1.96	1.66	5.80	0.66
$L5$	3.06	3.19	10.69	0.76
$L6$	3.11	2.57	6.15	0.75
$S1$	0.50	0.46	10.65	0.81
$S2$	1.61	1.09	8.22	0.64
$S3$	3.07	2.45	14.65	0.94
$S4$	3.40	3.48	22.15	1.32
$S5$	3.75	2.16	7.23	0.58

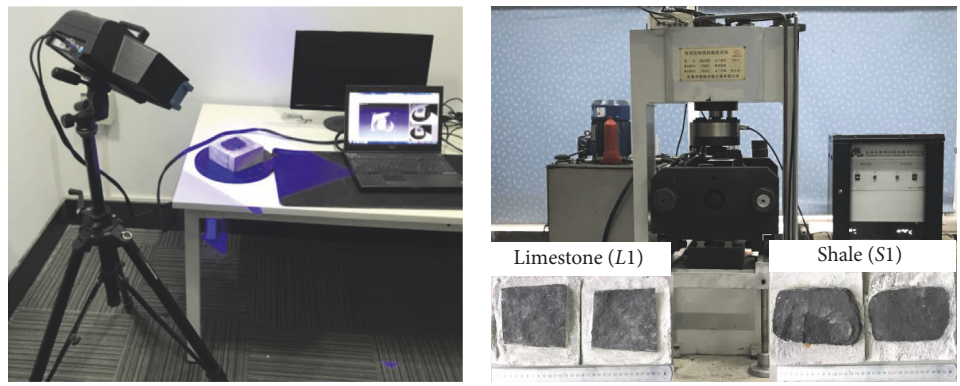

(a) (b)

Figure 10: (a) Data acquisition and (b) direct shear tests for rock discontinuity specimens.

proposed method and the back analysis method is observed. The back analysis method based on direct shear tests for JRC calculation is widely used in engineering practice [15]. According to (16), a strong correlation clearly exists between the shear strength (τ) and the JRC values (via back analysis). Therefore, to investigate the correlation of I_R with the shear strength of discontinuities, in this study, we analyzed the correlation between the values of I_R and JRC (via back analysis). Specifically, we borrowed seventy-four profile data and shear test results from literature to directly verify the validity of the proposed method. Additionally, 3D scanning and shear tests were performed on the eleven discontinuity specimens, also indicating a strong correlation between I_R and the shear strength of the discontinuities. However, to obtain a general applicable correlation between I_R and the shear strength for 3D discontinuities, the data from eleven discontinuity specimens may not suffice. Therefore, to further study the shear strength model that considers I_R, we need more discontinuity surface data and corresponding shear test results.

(2) Anisotropy and Sampling Interval Effects of I_R. Taking $L1$ as an example, the anisotropy and sampling interval effects are studied to further determine their impacts on the I_R estimation results. Twenty-four shear directions at intervals of 15° from 0° to 360° are considered to study the anisotropy effect of I_R (Figure 11(b)). Finally, the values of I_R for the 3D models of $L1$ with different values of D (e.g., 0.3, 0.5, 1, 3, and 5 mm) are calculated.

The results are shown in Figure 13 (the large rectangle is an enlarged view of the small rectangle), which indicates that the anisotropy and sampling interval effects can be observed in the 3D roughness estimation results based on I_R. Specifically, the roughness estimation results of the same discontinuity model may not be equal in different shear directions. Additionally, the I_R values of a discontinuity in the same shear direction generally increase with decreasing D. To qualitatively evaluated the variation of I_R in percentage for different D intervals, we calculate the maximum variation rate (named δ) for different direction using equation: $\delta = (I_{R(D=0.3\,\text{mm})} - I_{R(D=5\,\text{mm})})/I_{R(D=5\,\text{mm})}$, where $I_{R(D=0.3\,\text{mm})}$ and $I_{R(D=5\,\text{mm})}$ represent I_R values of $L1$ with $D = 0.3$ mm and $D = 5$ mm, respectively. The results are shown in Table 4. Additionally, the International Society for Rock Mechanics (ISRM) suggested that a discontinuity surface can be measured with $D < 0.5$ mm [35], and $D = 0.3$ mm was adopted by some researchers [14, 15, 26]. To be convenient for comparing with other methods, integrating the efficiency with the accuracy for I_R estimation, we propose a sampling interval D of 0.3 mm in the present study.

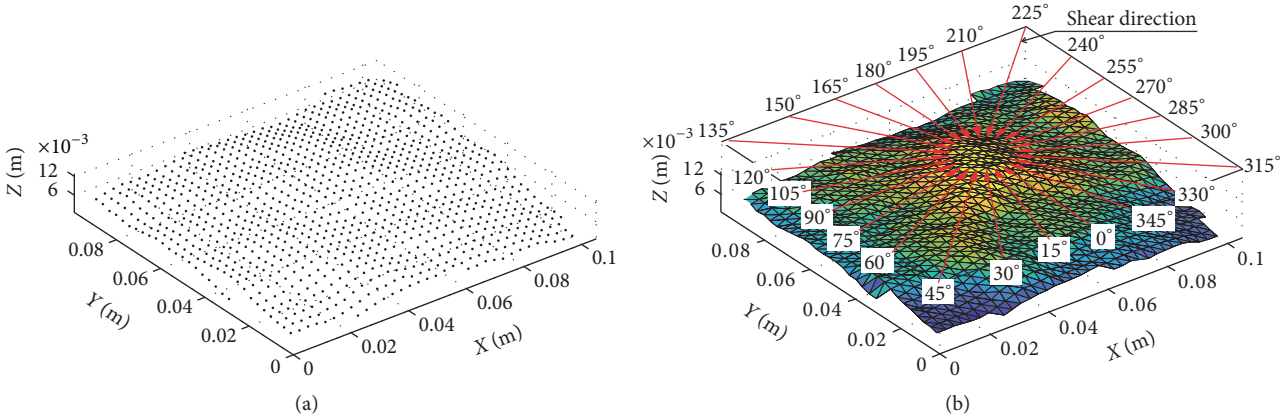

Figure 11: Modeling of discontinuity $L1$ (D = 3 mm): (a) point cloud of the discontinuity surface; (b) discontinuity surface with triangles.

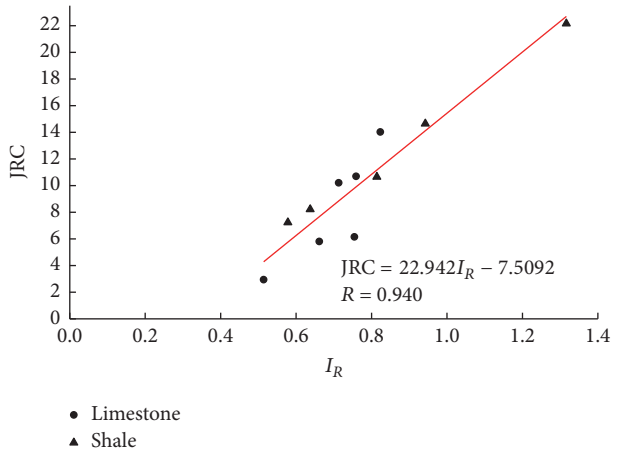

Figure 12: Correlation between I_R and JRC across the eleven discontinuity specimens.

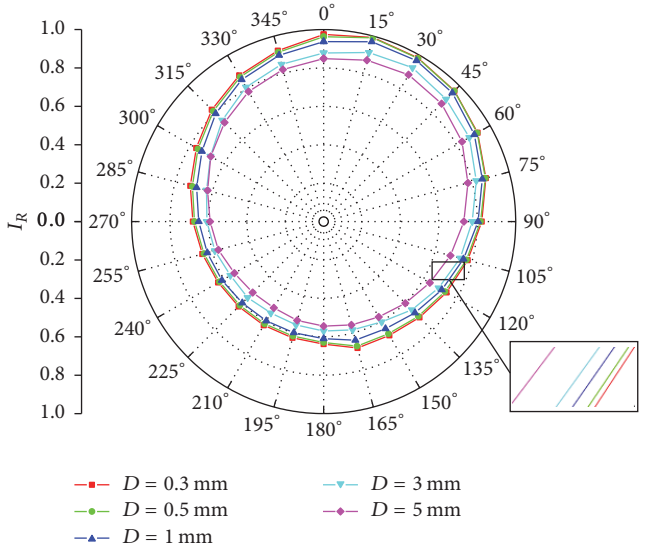

Figure 13: I_R values of the $L1$ models with different D values with respect to different shear directions.

Table 4: I_R variation rate δ for $L1$ in different directions.

Direction (°)	δ (%)
0	14.80
15	14.11
30	11.38
45	10.94
60	11.28
75	12.44
90	12.74
105	13.58
120	15.76
135	17.38
150	19.24
165	22.28
180	17.17
195	17.68
210	20.21
225	19.76
240	18.08
255	15.25
270	15.11
285	14.87
300	12.81
315	12.86
330	12.38
345	12.39

4.3. Comparison Analyses

(1) Comparison with the Parameter Z_2. For comparative analysis of the effectiveness of the 2D roughness estimation based on I_R, the seventy-four profiles are chosen to study. After calculating the Z_2 value of each profile model with D = 0.25 mm, we analyzed the relation between the values of Z_2 and JRC of these profiles. The distribution of Z_2 in relation to the JRC values for the seventy-four profiles is plotted in Figure 14. Additionally, the linear correlation coefficient (R)

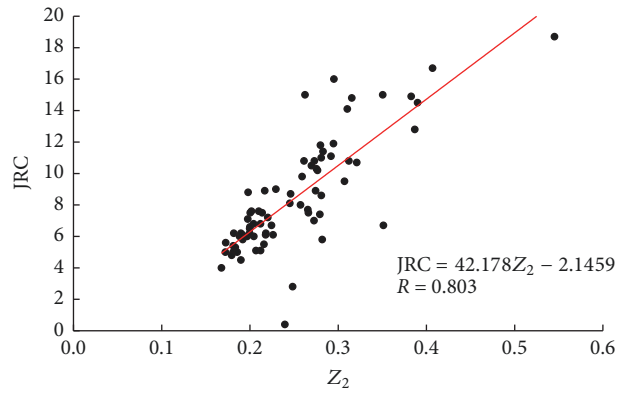

FIGURE 14: Distribution of Z_2 in relation to JRC for the seventy-four profiles (D = 0.25 mm).

between Z_2 and JRC is 0.803. Comparing Figures 14 and 7(b), the linear correlation between I_R and JRC is better than that of Z_2 and JRC across the seventy-four profiles.

(2) Comparison with Grasselli's Method. The roughness results for the eleven discontinuity specimens that were estimated using $\theta^*{}_{\max}/(C_G + 1)$ and I_R are compared and can also be used as evidence of the rationality of I_R. Based on Grasselli's method, the roughness of the eleven specimen models (D = 0.3 mm) was evaluated with respect to the twenty-four shear directions, and the results are partly shown in Figure 15. In addition, the plot of $\theta^*{}_{\max}/(C_G + 1)$ versus JRC for the eleven specimen models is shown in Figure 16. A comparison of Figures 16 and 12 shows that the linear correlation between I_R and JRC is clearly stronger than that between $\theta^*{}_{\max}/(C_G + 1)$ and JRC across the eleven specimens.

5. Summary and Conclusions

This study attempts to obtain a roughness parameter that is closely related to the shear strength of discontinuities. First, the shear failure mechanisms of the ITD models are analyzed based on the RTD models from Patton. Second, a formula (see (10)) for estimating the shear strength of a triangle within a discontinuity surface is derived. Finally, (15) with $\phi_b = 30^\circ$ and $\lambda = 3$ is proposed as an empirical equation for calculating I_R. The calculation of I_R using (15) is an application of (10). According to the definition and calculation of I_R, the parameter I_R has a clear mechanical basis and is closely related to the shear strength of discontinuities. Additionally, I_R of a discontinuity can be calculated based on its point cloud obtained from 3D laser scanning.

The computational processes and estimation effects of the proposed method are presented using several applications. Specifically, the seventy-four typical profiles and the eleven discontinuities are analyzed using the proposed method. These applications show that the discontinuity roughness estimated by both 2D and 3D I_R demonstrates the anisotropy and sampling interval effects. In addition, the I_R values show a strong linear correlation with the corresponding JRC values for the seventy-four profiles and eleven discontinuities.

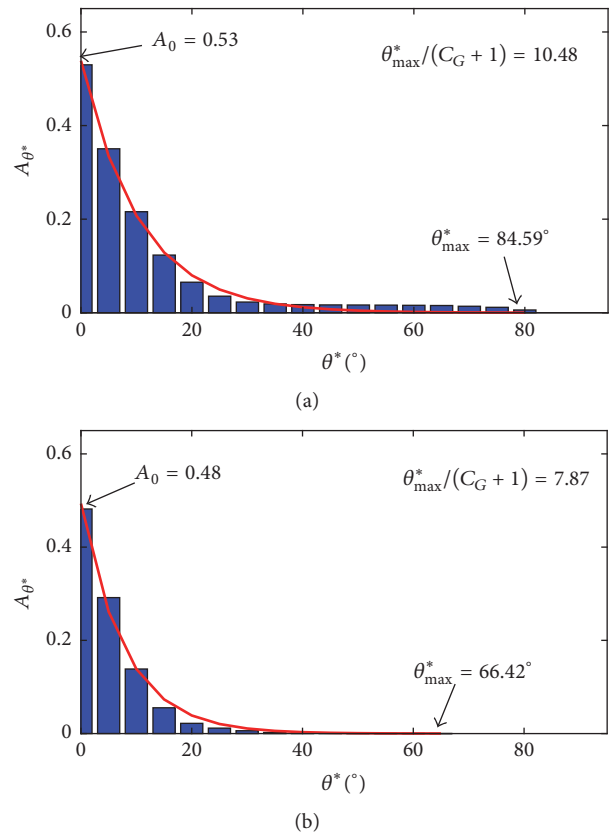

FIGURE 15: Histograms and corresponding fitting curves of A_{θ^*}-θ^* for (a) $L1$ and (b) $L2$ with respect to the 90° shear direction (D = 0.3 mm).

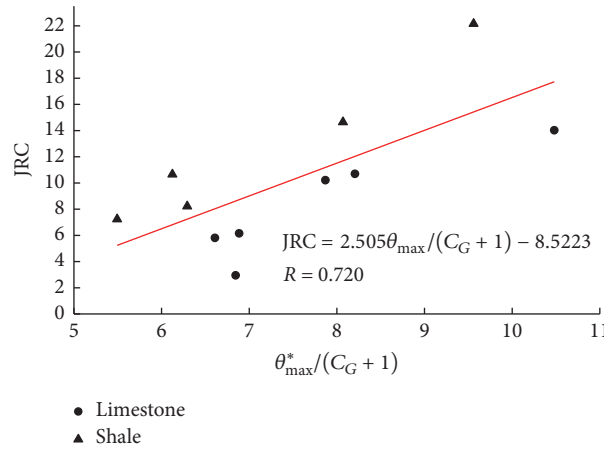

FIGURE 16: Correlation between $\theta^*{}_{\max}/(C_G + 1)$ and JRC across the eleven discontinuity specimens.

Comparison analyses are performed to study the use and robustness of the proposed method. For the seventy-four profiles, the linear correlation between the I_R and JRC is better than that between Z_2 and JRC. Additionally, for the eleven discontinuity specimens, the linear correlation between I_R and JRC is also stronger than that between $\theta^*{}_{\max}/(C_G + 1)$ and JRC. Therefore, the comparison analyses

indicate that a close correlation exists between I_R and the shear strength of discontinuities.

Conflicts of Interest

The authors declare that there are no conflicts of interest regarding the publication of this paper.

Acknowledgments

This work was funded by the National Key R&D Program of China (2017YFC1501305) and the Key National Natural Science Foundation of China (no. 41230637). This financial support is gratefully appreciated.

References

[1] N. Barton, "Review of a new shear-strength criterion for rock joints," *Engineering Geology*, vol. 7, no. 4, pp. 287–332, 1973.

[2] N. Barton and V. Choubey, "The shear strength of rock joints in theory and practice," *Rock Mechanics. Felsmechanik Mécanique des Roches*, vol. 10, no. 1-2, pp. 1–54, 1977.

[3] H. S. Lee, Y. J. Park, T. F. Cho, and K. H. You, "Influence of asperity degradation on the mechanical behavior of rough rock joints under cyclic shear loading," *International Journal of Rock Mechanics and Mining Sciences*, vol. 38, no. 7, pp. 967–980, 2001.

[4] R. Kumar and A. K. Verma, "Anisotropic shear behavior of rock joint replicas," *International Journal of Rock Mechanics and Mining Sciences*, vol. 90, pp. 62–73, 2016.

[5] R. W. Zimmerman and G. S. Bodvarsson, "Hydraulic conductivity of rock fractures," *Transport in Porous Media*, vol. 23, no. 1, pp. 1–30, 1996.

[6] H. S. Lee and T. F. Cho, "Hydraulic characteristics of rough fractures in linear flow under normal and shear load," *Rock Mechanics and Rock Engineering*, vol. 35, no. 4, pp. 299–318, 2002.

[7] N. O. Myers, "Characterization of surface roughness," *Wear*, vol. 5, no. 3, pp. 182–189, 1962.

[8] R. S. Sayles and T. R. Thomas, "The spatial representation of surface roughness by means of the structure function: A practical alternative to correlation," *Wear*, vol. 42, no. 2, pp. 263–276, 1977.

[9] S. M. El-Soudani, "Profilometric analysis of fractures," *Metallography*, vol. 11, no. 3, pp. 247–336, 1978.

[10] R. Tse and D. M. Cruden, "Estimating joint roughness coefficients," *International Journal of Rock Mechanics and Mining Sciences & Geomechanics Abstracts*, vol. 16, no. 5, pp. 303–307, 1979.

[11] N. H. Maerz, J. A. Franklin, and C. P. Bennett, "Joint roughness measurement using shadow profilometry," *International Journal of Rock Mechanics and Mining Sciences & Geomechanics Abstracts*, vol. 27, no. 5, pp. 329–343, 1990.

[12] X. Yu and B. Vayssade, "Joint profiles and their roughness parameters," *International Journal of Rock Mechanics and Mining Sciences*, vol. 28, no. 4, pp. 333–336, 1991.

[13] Z. Yang, S. C. Lo, and C. C. Di, "Reassessing the joint roughness coefficient (JRC) estimation using Z_2," *Rock Mechanics and Rock Engineering*, vol. 34, no. 3, pp. 243–251, 2001.

[14] G. Grasselli, J. Wirth, and P. Egger, "Quantitative three-dimensional description of a rough surface and parameter evolution with shearing," *International Journal of Rock Mechanics and Mining Sciences*, vol. 39, no. 6, pp. 789–800, 2002.

[15] G. Grasselli and P. Egger, "Constitutive law for the shear strength of rock joints based on three-dimensional surface parameters," *International Journal of Rock Mechanics and Mining Sciences*, vol. 40, no. 1, pp. 25–40, 2003.

[16] B. S. A. Tatone and G. Grasselli, "A method to evaluate the three-dimensional roughness of fracture surfaces in brittle geomaterials," *Review of Scientific Instruments*, vol. 80, no. 12, Article ID 125110, 2009.

[17] B. S. A. Tatone and G. Grasselli, "An investigation of discontinuity roughness scale dependency using high-resolution surface measurements," *Rock Mechanics and Rock Engineering*, vol. 46, no. 4, pp. 657–681, 2013.

[18] J. Ye, R. Yong, Q.-F. Liang, M. Huang, and S.-G. Du, "Neutrosophic Functions of the Joint Roughness Coefficient and the Shear Strength: A Case Study from the Pyroclastic Rock Mass in Shaoxing City, China," *Mathematical Problems in Engineering*, vol. 2016, Article ID 4825709, 2016.

[19] T. Belem, F. Homand-Etienne, and M. Souley, "Quantitative parameters for rock joint surface roughness," *Rock Mechanics and Rock Engineering*, vol. 33, no. 4, pp. 217–242, 2000.

[20] G. Zhang, M. Karakus, H. Tang, Y. Ge, and L. Zhang, "A new method estimating the 2D Joint Roughness Coefficient for discontinuity surfaces in rock masses," *International Journal of Rock Mechanics and Mining Sciences*, vol. 72, pp. 191–198, 2014.

[21] Y.-H. Lee, J. R. Carr, D. J. Barr, and C. J. Haas, "The fractal dimension as a measure of the roughness of rock discontinuity profiles," *International Journal of Rock Mechanics and Mining Sciences & Geomechanics Abstracts*, vol. 27, no. 6, pp. 453–464, 1990.

[22] H. Xie, J.-A. Wang, and M. A. Kwaśniewski, "Multifractal characterization of rock fracture surfaces," *International Journal of Rock Mechanics and Mining Sciences*, vol. 36, no. 1, pp. 19–27, 1999.

[23] P. H. S. W. Kulatilake, P. Balasingam, J. Park, and R. Morgan, "Natural rock joint roughness quantification through fractal techniques," *Geotechnical and Geological Engineering*, vol. 24, no. 5, pp. 1181–1202, 2006.

[24] F. D. Patton, "Multiple modes of shear failure in rock," in *Proceedings of the 1st ISRM Congress, International Society for Rock Mechanics*, pp. 509–513, 1966.

[25] Z.-Y. Yang, A. Taghichian, and G.-D. Huang, "On the applicability of self-affinity concept in scale of three-dimensional rock joints," *International Journal of Rock Mechanics and Mining Sciences*, vol. 48, no. 7, pp. 1173–1187, 2011.

[26] C.-C. Xia, Z.-C. Tang, W.-M. Xiao, and Y.-L. Song, "New peak shear strength criterion of rock joints based on quantified surface description," *Rock Mechanics and Rock Engineering*, vol. 47, no. 2, pp. 387–400, 2014.

[27] J. C. Jaeger, "Friction of Rocks and Stability of Rock Slopes," *Géotechnique*, vol. 21, no. 2, pp. 97–134, 1971.

[28] J. P. Pereira and M. H. de Freitas, "Mechanisms of shear failure in artificial fractures of sandstone and their implication for models of hydromechanical coupling," *Rock Mechanics and Rock Engineering*, vol. 26, no. 3, pp. 195–214, 1993.

[29] D. H. Kim, I. Gratchev, and A. Balasubramaniam, "Determination of joint roughness coefficient (JRC) for slope stability analysis: A case study from the Gold Coast area, Australia," *Landslides* , vol. 10, no. 5, pp. 657–664, 2013.

[30] K. Develi, T. Babadagli, and C. Comlekci, "A new computer-controlled surface-scanning device for measurement of fracture surface roughness," *Computers & Geosciences*, vol. 27, no. 3, pp. 265–277, 2001.

[31] D.-S. Bae, K.-S. Kim, Y.-K. Koh, and J.-Y. Kim, "Characterization of joint roughness in granite by applying the scan circle technique to images from a borehole televiewer," *Rock Mechanics and Rock Engineering*, vol. 44, no. 4, pp. 497–504, 2011.

[32] N. Fardin, O. Stephansson, and L. Jing, "The scale dependence of rock joint surface roughness," *International Journal of Rock Mechanics and Mining Sciences*, vol. 38, no. 5, pp. 659–669, 2001.

[33] H. Tang, Y. Ge, L. Wang, Y. Yuan, L. Huang, and M. Sun, "Study on estimation method of rock mass discontinuity shear strength based on three-dimensional laser scanning and image technique," *Journal of Earth Science*, vol. 23, no. 6, pp. 908–913, 2012.

[34] S. Bandis, *Experimental Studies of Scale Effects on Shear Strength, and Deformation of Rock Joints [Ph. D. Thesis]*, University of Leeds, Leeds, England, 1980.

[35] R. Ulusay, *The ISRM Suggested Methods for Rock Characterization, Testing and Monitoring: 2007-2014*, Springer International Publishing, Cham, Switzerland, 2015.